

Non-linear imaging techniques visualize the lipid profile of *C. elegans*

Meropi Mari^{1,2*}, Barbara Petanidou^{1,3}, Konstantinos Palikaras², Costas Fotakis^{1,3}, Nektarios Tavernarakis^{2,4}, George Filippidis¹

¹Institute of Electronic Structure and Laser, Foundation for Research and Technology, Heraklion 71110, Crete, Greece

²Institute of Molecular Biology and Biotechnology, Foundation for Research and Technology, Heraklion 71110, Crete, Greece

³Physics Department, University of Crete, Heraklion 71003, Crete, Greece

⁴Medical School, University of Crete, Heraklion 71003, Crete, Greece

*Corresponding author: mmari@imbb.forth.gr Tel ++302811392125

ABSTRACT

The non-linear techniques Second and Third Harmonic Generation (SHG, THG) have been employed simultaneously to record three dimensional (3D) imaging and localize the lipid content of the muscular areas (ectopic fat) of *Caenorhabditis elegans* (*C. elegans*). Simultaneously, Two-Photon Fluorescence (TPEF) was used initially to localize the stained lipids with Nile Red, but also to confirm the THG potential to image lipids successfully. In addition, GFP labelling of the somatic muscles, proves the initial suggestion of the existence of ectopic fat on the muscles and provides complementary information to the SHG imaging of the pharynx. The ectopic fat may be related to a complex of pathological conditions including type-2 diabetes, hypertension and cardiovascular diseases. The elucidation of the molecular path leading to the development of metabolic syndrome is a vital issue with high biological significance and necessitates accurate methods competent of monitoring lipid storage distribution and dynamics *in vivo*. THG microscopy was employed as a quantitative tool to monitor the lipid accumulation in non-adipose tissues in the pharyngeal muscles of 12 unstained specimens while the SHG imaging revealed the anatomical structure of the muscles. The ectopic fat accumulation on the pharyngeal muscles increases in wild type (N2) *C. elegans* between 1 and 9 days of adulthood. This suggests a correlation of the ectopic fat accumulation with the aging. Our results can provide new evidence relating the deposition of ectopic fat with aging, but also validate SHG and THG microscopy modalities as new, non-invasive tools capable of localizing and quantifying selectively lipid accumulation and distribution.

KEYWORD LIST

THG, SHG, non-linear phenomena, imaging, *C. elegans*, ectopic fat accumulation

1. INTRODUCTION

There is a variety of fluorescent based methods applied to the study of lipid metabolism. Fixation and staining or fluorescence imaging of live worms using dye feeding are the most popular fluorescent based methods. Nile Red¹, BODIPY², and Sudan black³ are the most efficient lipid stains. However, labeling often interferes with the normal function of the biomolecules and it may impact the physical and chemical environment *in vivo*. Consequently, fast, non-invasive, label-free microscopy methods are necessary to achieve accurate imaging and quantification of the lipid content.

Previous studies in *Drosophila* demonstrate how differential interference contrast (DIC) microscopy provides label-free imaging of lipid droplets *in vivo*^{4,5}. The primary drawback of DIC is that it is limited to a few droplets at a film and has a shallow penetration depth. Due to this shallow penetration depth, a mechanical sample compression is needed to reduce the thickness of the sample, and this external force may affect the cellular structure or smash it.

One label-free method is the Coherent anti-Stokes Raman scattering (CARS) microscopy that has been successfully employed to record *C. elegans* lipid profile⁶. This technique is valuable and efficient due to its chemical specificity, but it is costly as it requires two tightly synchronized and perfectly aligned laser beams⁷. CARS measurements lack efficient contrast due to strong autofluorescence, as well as due to non-resonant signal arising from any objects or the surrounding solvent. This limits the image contrast as well as the spectral sensitivity of this method⁸. Furthermore, Stimulated Raman Scattering (SRS) originates from the chemical contrast of intrinsic Raman vibrational frequencies providing better quality images free of non-resonant background. SRS has been employed to monitor the fat storage of *C. elegans* mutants contributing to valuable information on fat metabolism regulated by genes⁹. Nevertheless, the proper tuning of two synchronized beams is required for the SRS measurements¹⁰.

SHG and THG are coherent non-linear scattering phenomena. SHG signal originates from non-centrosymmetric molecules and provides knowledge related to the orientation and organization of structures that lack inversion symmetry¹¹. Such structures in tissues are myosin thick filaments¹², collagen¹³ or lipid membranes¹⁴.

THG is sensitive to local differences in third-order non-linear susceptibility $\chi^{(3)}$, refractive index and dispersion. Under tight focusing conditions, the THG signal increases upon beam focusing on the interface between two optically different materials. THG is a powerful non-invasive imaging technique able to reveal the anatomic features of many model organisms among them is the *C. elegans*¹⁵. THG requires a single beam and is efficient of recording cellular processes *in vivo*¹⁶, but also *in vitro* combined with further non-linear modalities¹⁷.

Recent studies have proved that THG is capable of revealing the morphology of unstained tissues¹⁸ as well as lipid droplets in tissues¹⁹ and cells²⁰. THG imaging has identified the different developmental stages of *C. elegans*^{21,22} and has monitored the progress of the embryonic development^{23,24}. In addition, the detection of lipid body structures in mouse embryos provides valuable knowledge concerning the energetic status of preimplantation of the embryos as well as their blastomere equivalence²⁵. Furthermore, previous studies²⁶ have visualized successfully the intestinal lipid droplets which are a part of the adipose tissue in *C. elegans*. Simultaneously, TPEF was performed using various labels²⁶, to verify the success of the THG imaging of the lipids.

In this work, THG imaging microscopy has been operated as a diagnostic tool to detect and quantify the ectopic accumulation of lipids in non-adipose tissues and particularly on pharyngeal muscles. The model organism *C. elegans* has been utilized as a resourceful model organism²⁷ for our study.

2. MATERIALS AND METHODS

2.1 Experimental set-up

Our experimental set-up can be found in previous work of the group²⁸. The laser source exploited is a 1028nm pulsed femtosecond laser (200fs, 50MHz). This beam is passing through a modified Nikon upright microscope (Eclipse ME600D). The control of the laser power is adjusted by neutral density filters (New Focus, Newport Corp.). The sample scanning is achieved through the operation of a set of galvanometric mirrors (Cambridge Technology) that are placed on the microscope before the telescopic system. The beam radius control is important in order to fulfill the rear aperture of the objective lens, thus the maximum field of view along with the tight focusing are achieved, within the limits of the lens. A motorized translation stage (Standa Ltd., Lithuania; 1 μ m minimum step) defines the focal plane, while the beam is tightly focused by an objective lens of high numerical aperture (Carl Zeiss, C-Achroplan 32x, NA 0.85, water immersion). A pair of thin circular coverslips (70 μ m, ϕ 35 mm, Marienfeld), divided by a 100 μ m thick spacer, are used as sample holders. The aberration ring of the objective (0-0.17mm) is suitable for the thickness of the glass coverslips utilized. A condenser lens (Carl Zeiss, PlanNeofluar, 40x, 0.75 NA, air immersion) is used to collect the multimodal signals (THG or SHG) in the transmission mode. The NA of the objective and condenser are similar and the condenser is validated to have high UV transmission for the THG light (343nm).

The non-linear signals (THG and TPEF or SHG) are simultaneously produced at the focal volume and are detected in the transmission or reflection mode, respectively. This quality of our apparatus allows the performance of co-localization measurements. The data acquisition as well as the sample scanning is controlled by a LabVIEW interface, designed according the experiment requirements. Two photomultipliers (PMT Hamamatsu) wired to the computer, are employed to detect the transmitted and reflected signals. Appropriate filters are placed before the detection scheme to eliminate the laser beam and collect the selected signal (THG, SHG or TPEF). A 514nm bandpass filter (CVI F03-514.5) was placed at the PMT to detect the SHG signal. For the collection of THG signals a colored glass filter (U 340-Hoya) is set in front of the second PMT. For the TPEF measurements, a short pass filter (SPF 700 nm, CVI) eliminates any reflection from the fundamental beam, while a bandpass filter (640 nm / 40 nm, Chroma) is used for the detection of Nile Red fluorescence and a long pass filter (520nm, CVI) for the GFP fluorescence detection.

For this presented work, the 500 x 500 pixel images of all modalities are averaged 30 times to improve the signal to noise ratio. The total acquisition time for each image was 33 seconds. All the figures are z-projections of slice images separated by a 2 μ m distance. For all the figures, the pixel size is 0.27 μ m. For the reconstruction and processing of the figures, Image

J was employed (NIH, <http://imagej.nih.gov/ij/>).

2.2 *C. elegans*: Strains and Maintenance - Lipid staining

C. elegans worms were kept at 20°C and maintained on standard NGM plates seeded with *E. coli* OP50 bacteria. Bristol N2: wild-type strain used in the study.

2.2.1 Nile Red staining

NGM plates were seeded with OP50 *E. coli* bacteria and allowed to dry overnight at room temperature. L4- stage worms were incubated on plates seeded with OP50 bacteria and transferred to fresh plates every other day until they reached day 1 and day 9 of adulthood. Worms were fixed for 5 minutes in 3 mL cold (-20°C) methanol. 2mL of PBTw (PBS with 0.1% Tween-20) were added, and the tubes were centrifuged for 2 minutes at 300 rpm to eliminate the supernatant. Finally, worms were washed twice in PBTw. After fixation worms were stained for 20 minutes in 10 mM Nile Red (Sigma Aldrich Corp.), added from a stock solution of 50 mM Nile Red diluted in 100% ethanol.

2.2.2 GFP on the muscles

For the set of experiments with GFP in the somatic muscles the animals used, were delivered stained and went through the standard procedures. The strain used was the SJ4103:N2;*Ex[p_{myo-3} GFP]*.

2.2.3 Unstained worms

Prior to imaging, worms were collected with M9 isotonic buffer; 22 mM KH₂PO₄ (Merck cat.no. 1.04873.1000), 42 mM Na₂HPO₄ (Merck cat. no. 1.06586.0500), 85 mM NaCl (Merck cat. no.1.06404.1000), and 1 mM MgSO₄ (Sigma cat. no. M-7506). Dissolve 3 g KH₂PO₄, 6 g Na₂HPO₄, 5 g NaCl, and 1 m: 1 M MgSO₄ in 1 L distilled water. Autoclave and keep it refrigerated. Then, worms were washed several times with M9 buffer to remove any bacteria. Finally, the worms were immobilized with 10 mM sodium azide buffer at final concentration. The immobilization worms are examined microscopically.

3. RESULTS AND DISCUSSION

THG comprises a valuable diagnostic tool that provides unique morphological information for various samples. In combination with SHG reciprocal information can be extracted concerning the musculature as well as the internal structures. Previous work has revealed and quantified²⁶ the adipose fat of the intestine of *C. elegans*. In this study our interest is focused on the non-adipose fat of the nematode which is mainly deposited in the pharyngeal muscles. This lipid accumulation is visualized and quantified precisely through the use of non-invasive imaging techniques.

THG signals arise from various discontinuities especially in the anterior part of the animal. Figure 1 is a montage of z-projections (of all slices) of each signal separately and their multi-modal image. Figure 1(a) reveals the adipose fat in the vulva region of a 1 day young wild type animal. There is an outstanding co-localization of the stained lipids with Nile Red revealed by TPEF(red) and the THG image (green) arising mainly from the lipids, resulting in yellow structures. Figure 1(b) depicts the co-localization of the lipids in the area of the head. This is an area that the adipose fat is quite limited to the outer epidermal layers and the main lipid structures belong to the non-adipose fat (ectopic fat). The THG reveals also the isthmus that connects the two bulbs, the grinder of the terminal bulb as well as the cuticle of the animal. The dyed lipid droplets of the head (red) are well co-localized with the THG signals originating from the lipids (green) resulting in the yellow structures along the lumen. Figure 1(c) similar measurements are performed on the tail of the young wild type animal. THG (green) reveals the anatomical features of the tail, such as the cuticle and mainly the lipids, while the TPEF (red) depicts only the lipids of the tail which overlap with the THG lipid structures resulting in the yellow result.

We investigate the feasibility of THG to localize the ectopic fat accumulation on muscle cells. Whereas *C. elegans* lacks of dedicated adipose tissues, its intestine and hypodermis serve as the main lipid storage sites. The head region and especially the area between the two bulbs of the pharynx is the only part of the animal where the intestinal lipids are excluded. The tail region contains lipids but also contains products of metabolism that are capable of giving rise to THG signals. Consequently, the head area appears to be the most suitable. This is critical for the following measurements of the THG signal quantification that has to exclude any signal coming from the adipose tissue. All the ectopic fat quantification is performed on the region between the two bulbs of the pharynx in the head.

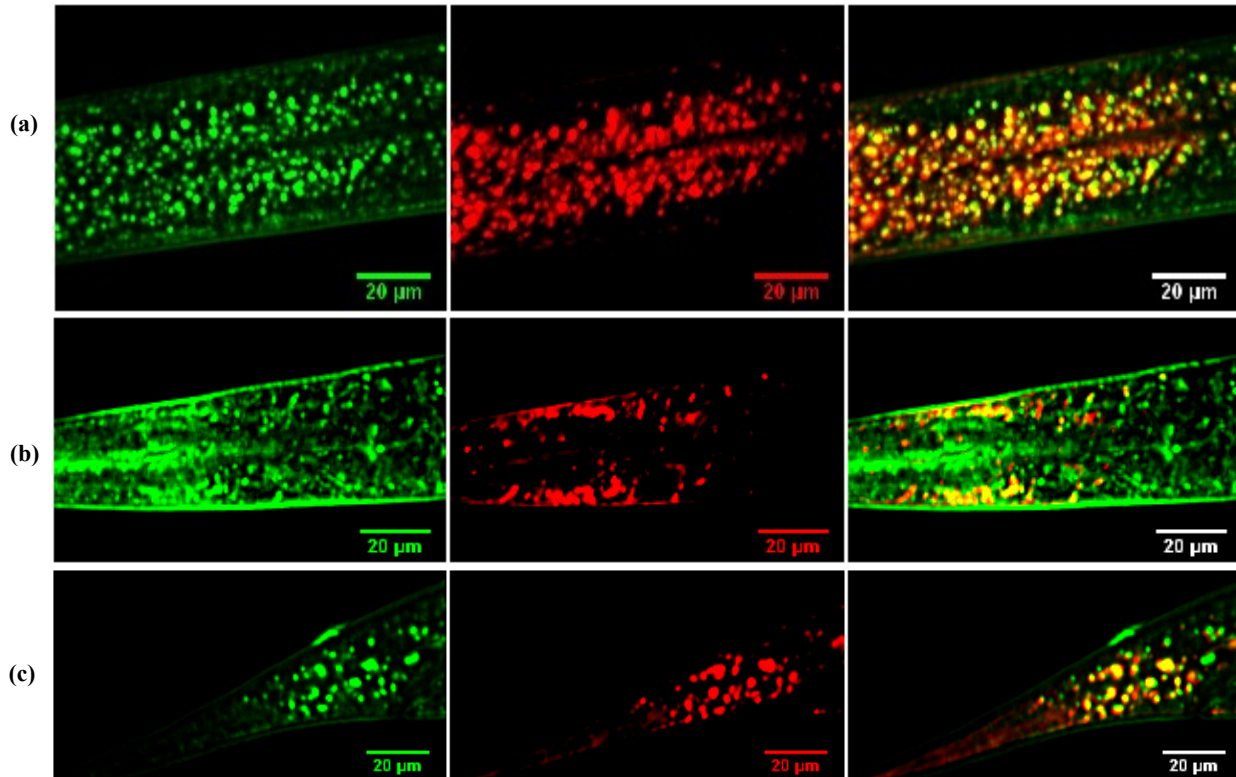


Figure 1: Non-linear imaging of 1 day old wild type *C. elegans*; THG (green), TPEF (red), merge of the two signals resulting in yellow overlapping lipid droplets. (a) vulva region with high content of adipose fat, z-projection of 27 slices, (b) pharynx containing ectopic fat, z-projection of 19 slices, (c) tail region, z-projection of 14 slices.

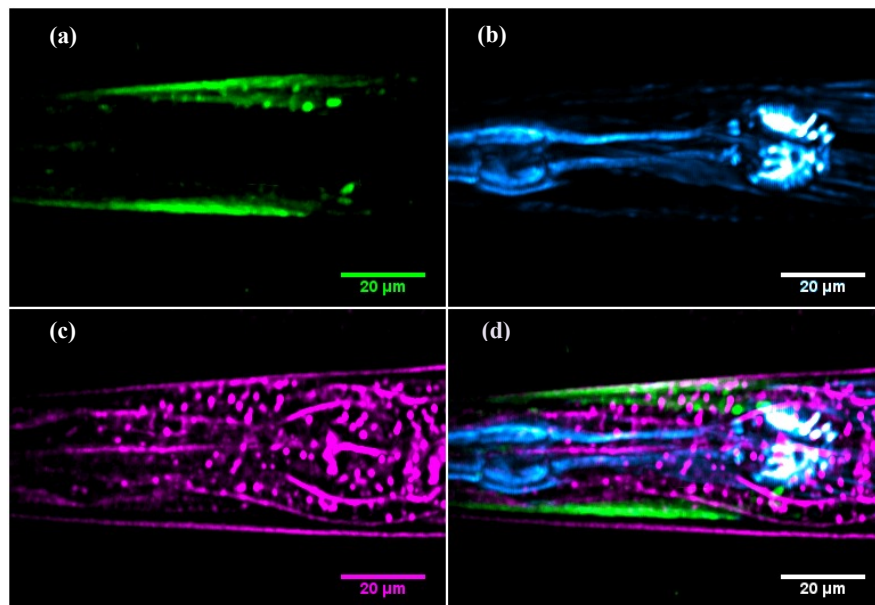


Figure 2: Z-projections of 22 slices of the pharynx of a 1 day old *C. elegans*; (a) TPEF (green) arising from the GFP stained somatic muscles, (b) SHG (cyan hot) revealing mainly the pharyngeal muscles of the head but also a few striated, (c) THG (magenta) images the anatomic features of the head and (d) is the multi-modal image of all three colours. Scale bar 20 μm .

Another set of experiments was performed to reveal the striated muscles of the head area and the lipid accumulation on them using GFP labelling in the somatic muscles. The pharyngeal muscles emanate strong SHG signal that obscures the relatively lower SHG signals of the striated muscles. The TPEF arising from the GFP stained somatic muscles depicts the location of the head muscles on the sides of the head (Figure 2(a), green). Simultaneously, the SHG signals from the pharyngeal but also the striated muscles are shown in Figure 2(b) (hot cyan). The THG signals (Figure 2c, magenda) reveal the anatomic features of the head with the lipid droplets to overwhelm. Finally, all the signals are merged in Figure 2(d) presenting the capability of our system to record simultaneously three different non-linear signals. All of the figures are z-projections to maximum intensity of 22 slices separated by 2 μ m.

The THG signal quantification requires the setting of a threshold on the obtained normalized slice images. Regions generating high levels of nonlinear signal, which are mainly corresponding to lipid droplets, are solely detected and isolated. Processing of images and thresholding are performed by using Image J. Normalized 8-bit slice images of the sample are thresholded using a constant threshold value. Only the highest 23.5% of the THG signals is quantified in a way that the generated stack of binary images represents exclusively the lipid droplets in the muscles (ectopic fat), while any other signals from the contour or the mouth and the lumen are either excluded or eliminated. Lipid content is measured by calculating the total pixel area of detected regions for all optical planes covering the total sample volume.

The total sum of the detected areas (in pixels) is calculated as a representative index of the total lipid content within the examined part of the pharynx region. Total lipid particle area measurements of these two different samples are compared by one sample t-test (SPSS, IBM Corp.). The total volume of the ectopic fat of each animal is calculated and averaged over a number of 12 animals for each age. Figure 3(a) presents the z-projection of 18 slices of THG imaging on the head of a 1 day old wild type unstained animal. Figure 3 (b) is the z-projection of all binary thresholded images that are included to the quantification. Figure 3 (c) depicts the mean number of pixels above intensity threshold of the total lipid content area in the head muscles of wild type animals of 1-day and 9-day old. The graph reveals the increase in the ectopic fat content along with the age progress of the animals. This difference is statistically significant ($P < 0.005$).

It is already reported that *C. elegans* adult hermaphrodite animals display an age-related increase in body size^{29,30} (length, width, and volume) between day 3 to day 14. For our experiments, only the lipids between the two bulbs are measured and quantified. All the areas of the young and the old animals were measured giving a 1.36:1 (old/young) volume ratio, according to which the fat content was normalized. The difference in the lipid area between the young and the old animals is still significant. These results indicate that THG modality could be used as a new nondestructive label-free diagnostic tool for the ectopic fat visualization and quantification in lipid biology research. By employing this technique, no external dyes are needed for staining the lipids. Moreover, complementary information can be obtained related to the anatomy and morphology of the muscles via the simultaneous detection of SHG signals.

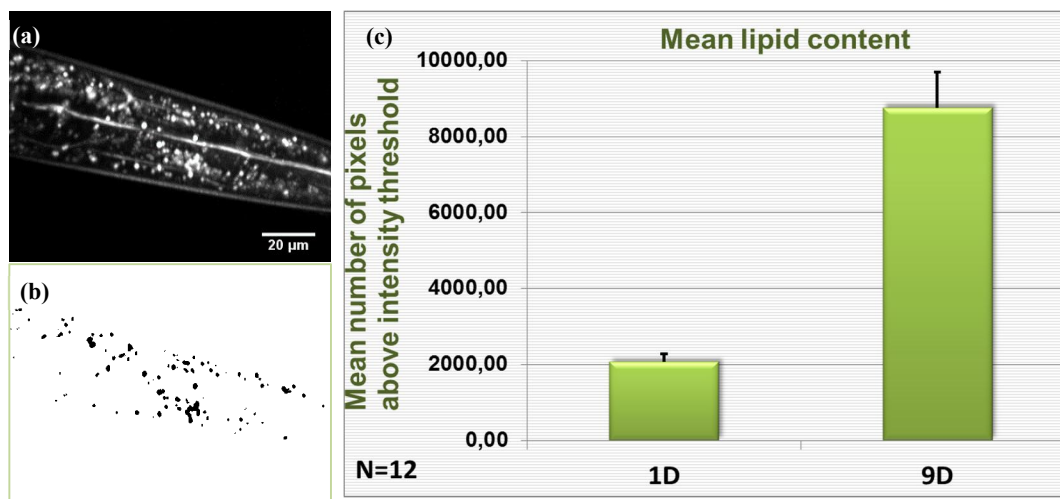


Figure 3: (a) Z-projection to maximum intensity of 18 slices; THG imaging of the head area of a 1 day old wild type (N2) animal. (b) Z-projection of all the binary thresholded slices. (c) Quantification of the mean total lipid area of 1-day-old and 9-day old wild-type (N2) animals, normalized with respect to the body size (n=12, error bars denote the standard error of the mean SEM).

4. CONCLUSIONS

Multiphoton microscopes are now commercially available and they can be easily upgraded for the detection of additional nonlinear signals (SHG, THG). Nonlinear microscopes are flexible and easy to use systems. A single femtosecond laser beam is required for the achievement of the measurements (TPEF, SHG, and THG); in contrast to other more complicated label free microscopy techniques such as CARS. These advantages facilitate the widespread adoption of nonlinear imaging microscopy and especially THG modality as a versatile, reliable, and easily accessible tool for lipid biology research. Nonlinear imaging microscopy methods are validated techniques for the in vivo imaging and localizing of subcellular biological structures and processes. The use of Nile Red guaranteed the success THG capability to image the ectopic fat. This was further reinforced by the use of the GFP staining in the somatic muscles of *C. elegans* which revealed the accumulation of ectopic fat on the somatic muscles. In this study, we show that THG can be used as a new diagnostic tool for the accurate visualization and quantification of ectopic fat accumulation in non-adipose tissues of *C. elegans* samples without the need of external dyes. We have achieved to visualize simultaneously the muscles and the lipid droplets distribution in the pharyngeal region of unstained wild-type *C. elegans* samples by employing SHG and THG imaging techniques. Our sample number was collected after multiple sets of experiments. By performing quantification of the collected THG signals a significant increase in the ectopic fat accumulation in older animals was detected. Changes of fat distribution in elderly animals could lead to lipotoxic effects, contributing to the disruption of tissue function during aging³¹. It is possible that free fatty acids (FFAs) or their metabolites trigger cell death or oxidative stress damaging cellular function^{32,33}. However, further studies are necessary to elucidate the link between ectopic fat accumulation and the process of aging.

ACKNOWLEDGMENTS

This work was supported by the FP7 projects "LASERLAB-EUROPE" (228334), the REGPOT-2012-2013-1 and the BIOSYS research project, Action KRIPIS, project No MIS-448301 (2013SE01380036) that was funded by the General Secretariat for Research and Technology, Ministry of Education, Greece and the European Regional Development Fund (Sectoral Operational Programme: Competitiveness and Entrepreneurship, NSRF 2007-2013)/ European Commission.

5. REFERENCES

- [1] Greenspan, P. and Fowler, S. D., "Spectrofluorometric studies of the lipid probe, Nile red," *Journal of Lipid Research* **26**(7), 781-789 (1985).
- [2] Mak, H. Y., Nelson, L. S., Basson, M., Johnson, C. D. & Ruvkun, G., "Polygenic control of *Caenorhabditis elegans* fat storage," *Nat. Genet.* **38**(3), 363-368 (2006).
- [3] Ashrafi, K. et al., "Genome-wide RNAi analysis of *Caenorhabditis elegans* fat regulatory genes," *Nature* **421**(6920), 268-272 (2003).
- [4] Welte, M. A. et al., "Developmental regulation of vesicle transport in *Drosophila* embryos: forces and kinetics," *Cell* **92**, 547-557 (1998).
- [5] Shubeita, G. T. et al., "Consequences of motor copy number on the intracellular transport of kinesin-1-driven lipid droplets," *Cell* **135**, 1098-1107 (2008).
- [6] Hellerer, T. et al., "Monitoring of lipid storage in *Caenorhabditis elegans* using coherent anti-Stokes Raman scattering (CARS) microscopy," *Proceedings of the National Academy of Sciences* **104**(37), 14658-14663 (2007).
- [7] Potma, E. O., Jones, D. J., Cheng, J. X., Xie, X. S. & Ye, J., "High-sensitivity coherent anti-Stokes Raman scattering microscopy with two tightly synchronized picosecond lasers," *Opt. Lett.* **27**(13), 1168-1170 (2002).

- [8] Cheng, J.X. and Xie, X. S., "Coherent Anti-Stokes Raman Scattering Microscopy: Instrumentation, Theory, and Applications," *The Journal of Physical Chemistry B* **108**(3), 827-840 (2004).
- [9] Wang, M. C., Min, W., Freudiger, C. W., Ruvkun, G. & Xie, X. S., "RNAi screening for fat regulatory genes with SRS microscopy," *Nature Methods* **8**(2), 135-138 (2011).
- [10] Lu, F.K. et al., "Multicolor stimulated Raman scattering (SRS) microscopy," *Molecular physics* **110**(15-16), 1927-1932 (2012).
- [11] Pelegati, V. B. et al., "Harmonic optical microscopy and fluorescence lifetime imaging platform for multimodal imaging," *Microscopy Research and Technique* **75**(10), 1383-1394 (2012).
- [12] Rehberg, M., Krombach, F., Pohl, U. & Dietzel, S., "Label-Free 3D Visualization of Cellular and Tissue Structures in Intact Muscle with Second and Third Harmonic Generation Microscopy," *PLoS ONE* **6**(11), e28237 (2011).
- [13] Cox, G. et al., "3-Dimensional imaging of collagen using second harmonic generation," *Journal of Structural Biology* **141**(1), 53-62 (2003).
- [14] Zhuo, S. et al., "Label-Free Imaging of Basement Membranes Differentiates Normal, Precancerous, and Cancerous Colonic Tissues by Second-Harmonic Generation Microscopy," *PLoS ONE* **7**(6), e38655 (2012).
- [15] Gualda, E. J. et al., "In vivo imaging of cellular structures in *Caenorhabditis elegans* by combined TPEF, SHG and THG microscopy," *Journal of Microscopy* **229**(1), 141-150 (2008).
- [16] Filippidis, G. et al., "In vivo imaging of cell morphology and cellular processes in *Caenorhabditis elegans* using non-linear phenomena," *Micron* **40**(8), 876-880 (2009).
- [17] Aptel, F. et al., "Multimodal nonlinear imaging of the human cornea," *Invest. Ophthalmol. Vis. Sci.* **51**, 2459-2465 (2010).
- [18] Oron, D. et al., "Depth-resolved structural imaging by third-harmonic generation microscopy," *Journal of Structural Biology* **147**(1), 3-11 (2004).
- [19] Debarre, D. et al., "Imaging lipid bodies in cells and tissues using third-harmonic generation microscopy," *Nature Methods* **3**(1), 47-53 (2006).
- [20] Zimmerley, M., Mahou, P., Débarre, D., Schanne-Klein, M.-C. & Beaurepaire, E., "Probing Ordered Lipid Assemblies with Polarized Third-Harmonic-Generation Microscopy," *Physical Review X* **3**(1), 011002 (2013).
- [21] Aviles-Espinosa, R. et al., "Third-harmonic generation for the study of *Caenorhabditis elegans* embryogenesis," *BIOMEDO* **15**(4), 046020-046020-046027 (2010).
- [22] Tserevelakis, G. J. et al., "Imaging *Caenorhabditis elegans* embryogenesis by third-harmonic generation microscopy," *Micron* **41**(5), 444-447 (2010).
- [23] Olivier, N., Aptel, F., Plamann, K., Schanne-Klein, M.C. & Beaurepaire, E., "Harmonic microscopy of isotropic and anisotropic microstructure of the human cornea," *Opt. Express* **18**(5), 5028-5040 (2010).
- [24] Tserevelakis, G. J., Filippidis, G., Megalou, E. V., Fotakis, C. & Tavernarakis, N., "Cell tracking in live *Caenorhabditis elegans* embryos via third harmonic generation imaging microscopy measurements," *BIOMEDO* **16**(4), 046019-046019-046016 (2011).
- [25] Kyvelidou, C. et al., "Following the course of pre-implantation embryo patterning by non-linear microscopy," *Journal of Structural Biology* **176**(3), 379-386 (2011).

- [26] Tserevelakis, G. J. et al., "Label-Free Imaging of Lipid Depositions in *C. elegans* Using Third-Harmonic Generation Microscopy," PLoS ONE **9**(1), e84431 (2014).
- [27] Vancoppenolle, B., Claeys, M., Borgonie, G., Tytgat, T. & Coomans, A., "Evaluation of fixation methods for ultrastructural study of *Caenorhabditis elegans* embryos," Microscopy Research and Technique **49**(2), 212-216 (2000).
- [28] Mari, M. et al., "Imaging ectopic fat deposition in *Caenorhabditis Elegnas* muscles using non linear microscopy, " Microscopy Research and Technique, in press (2015).
- [29] Bolanowski, M.A., Russell, R.L., Jacobson, L.A., "Quantitative measures of aging in the nematode *caenorhabditis elegans*. I. Population and longitudinal studies of two behavioral parameters," Mechanisms of Ageing and Development **15**, 2792295 (1981).
- [30] Croll, N.A. Smith, J.M., Zuckerman, B.M., "The aging process of the nematode *Caenorhabditis elegans* in bacterial and axenic culture," Experimental Aging Research **3**, 1752189 (1977).
- [31] Hemdon, L.A. et al., "Stochastic and genetic factors influence tissue-specific decline in ageing *C. elegans*," Nature **419**, 808–814 (2002).
- [32] Furuno, T. et al., "Roles of long chain fatty acids and carnitine in mitochondrial membrane permeability transition," Biochem. Pharmacol. **68**, 1037–1046 (2001).
- [33] Piro, S., Anello, M., Di Pietro, C., Lizzio, M.N., Patan, G., Rabuazzo, A.M., Vigneri, R., Purrello, F., Purrello, F., "Chronic exposure to free fatty acids or high glucose induces apoptosis in rat pancreatic islets: Possible role of oxidative stress, " Metabolism **51**, 1340–1347 (2002).